

Monolithic Discretization of Linear Thermoelasticity Problems via Adaptive Multimesh hp -FEM

P. Solin^{1,2*}, J. Cerveny², L. Dubcova², and D. Andrs^{1,2}

¹ University of Nevada, Reno, NV 89557, USA

² Institute of Thermomechanics

Academy of Sciences of Czech Republic, Dolejskova 5, Prague

e-mails: solin@unr.edu, jakub.cerveny@gmail.com, dubcova@gmail.com, andrsd@gmail.com

Abstract

In linear thermoelasticity models, the temperature T and the displacement components u_1, u_2 exhibit large qualitative differences: While T typically is very smooth everywhere in the domain, the displacements u_1, u_2 have singular gradients (stresses) at re-entrant corners and edges. The mesh must be extremely fine in these areas so that stress intensity factors are resolved sufficiently. Among the best available methods for this task is the exponentially-convergent hp -FEM. Note, however, that standard adaptive hp -FEM approximates all three fields u_1, u_2 and T on the same mesh, and thus it treats T as if it was singular at re-entrant corners as well. Therefore, large numbers of temperature degrees of freedom are wasted. This motivates us to approximate the fields u_1, u_2 and T on individual hp -meshes equipped with mutually independent hp -adaptivity mechanisms. In this paper we describe mathematical and algorithmic aspects of the novel adaptive multimesh hp -FEM, and demonstrate numerically that it performs better than standard adaptive h -FEM and hp -FEM.

1 Introduction

Linear thermoelasticity describes the behavior of elastic structures subject to moderate temperature changes [1, 2, 3, 4]. More complicated nonlinear models (not considered here) need to be employed to study the effects of large temperature variations such as the stability of concrete or steel constructions in fire [5, 6, 7, 8].

Traditionally, thermoelasticity problems have been solved using non-adaptive low-order methods (both finite elements and finite differences) that approximate all fields u_1, u_2 and T on the same mesh [1, 3]. More recently, one has employed operator splitting (OS) schemes to solve the elasticity and heat transfer processes more efficiently using individual meshes for u_1, u_2 and T [9]. However, OS schemes typically are non-adaptive, and moreover they are known to suffer from the loss of accuracy and/or stability caused by the transfer of data between meshes and/or by incomplete fixed point iteration [10, 11]. In this paper we propose a novel technique that makes it possible to solve thermoelasticity problems monolithically (without operator splitting and the associated problems), using an adaptive higher-order finite element discretization based on individual meshes for the fields u_1, u_2 and T .

The outline of the paper is as follows: In the rest of Section 1 we present the governing equations, boundary conditions and weak formulation. In Section 2 we describe the multimesh hp -FEM and discuss automatic adaptivity on multiple meshes. In Section 3 we present a model problem and compare the performance of adaptive hp -FEM (both standard and multimesh) with h -adaptive quadratic FEM.

*This work was supported by the Grant Agency of the Czech Republic project 102/07/0496, as well as by the Grant Agency of the Academy of Sciences of the Czech Republic project IAA100760702. The research of L. Dubcova was partly supported by the grant No. 48607 of the Grant Agency of the Charles University in Prague.

1.1 Plane-strain formulation of linear thermoelasticity

The plane-strain model of linear thermoelasticity inherits basic simplifying assumptions from the plane-strain elasticity model,

$$\varepsilon_{33} = \varepsilon_{13} = \varepsilon_{23} = 0. \quad (1)$$

Moreover, it assumes temperature-dependent strains in the form

$$\varepsilon_{ii} = \frac{\partial u_i}{\partial x_i} = \varepsilon_{ii,E} + \varepsilon_{ii,T} = \varepsilon_{ii,E} + \alpha(T - T_0), \quad 1 \leq i \leq 3 \quad (2)$$

(repeated indices do not imply Einstein summation). Here $\varepsilon_{ii,E}$, $\varepsilon_{ii,T}$, and ε_{ii} stand for the elastic, thermal, and total strains in the x_i -direction, respectively. By u_i we denote the displacement component in the x_i -direction, α is the thermal expansion coefficient, T the temperature, and T_0 a constant temperature corresponding to a stress-free initial configuration. The material is assumed to be isotropic. Recall that the stress component σ_{33} is nonzero in general.

Substituting assumptions (1), (2) into the basic stress-strain relation

$$\sigma_{ij} = \frac{E}{1+\nu} \varepsilon_{ij,E} + \frac{E\nu \sum_{k=1}^3 \varepsilon_{kk,E}}{(1-2\nu)(1+\nu)} \delta_{ij}, \quad 1 \leq i, j \leq 3, \quad (3)$$

we obtain a system of equations for the stress components,

$$\left. \begin{aligned} \sigma_{11} &= \frac{E}{(1-2\nu)(1+\nu)} [(1-\nu)\varepsilon_{11,E} + \nu(\varepsilon_{22,E} + \varepsilon_{33,E})] \\ &= \frac{E}{(1-2\nu)(1+\nu)} \left[(1-\nu) \frac{\partial u_1}{\partial x_1} + \nu \frac{\partial u_2}{\partial x_2} \right] - \frac{E\alpha(T-T_0)}{1-2\nu}, \\ \sigma_{22} &= \frac{E}{(1-2\nu)(1+\nu)} [(1-\nu)\varepsilon_{22,E} + \nu(\varepsilon_{11,E} + \varepsilon_{33,E})] \\ &= \frac{E}{(1-2\nu)(1+\nu)} \left[(1-\nu) \frac{\partial u_2}{\partial x_2} + \nu \frac{\partial u_1}{\partial x_1} \right] - \frac{E\alpha(T-T_0)}{1-2\nu}, \\ \sigma_{33} &= \frac{E}{(1-2\nu)(1+\nu)} [(1-\nu)\varepsilon_{33,E} + \nu(\varepsilon_{22,E} + \varepsilon_{11,E})], \\ &= \frac{E\nu}{(1-2\nu)(1+\nu)} \left(\frac{\partial u_1}{\partial x_1} + \frac{\partial u_2}{\partial x_2} \right) - \frac{E\alpha(T-T_0)}{1-2\nu}, \\ \sigma_{12} &= \frac{E}{2(1+\nu)} \varepsilon_{12,E} = \frac{E}{2(1+\nu)} \left(\frac{\partial u_1}{\partial x_2} + \frac{\partial u_2}{\partial x_1} \right). \end{aligned} \right\} \quad (4)$$

Here, E and ν stand for the Young modulus and Poisson number, respectively. Substituting the stresses σ_1 , σ_2 , and σ_{12} from (4) into the equilibrium equations

$$\left. \begin{aligned} \frac{\partial \sigma_{11}}{\partial x_1} + \frac{\partial \sigma_{12}}{\partial x_2} + f_1 &= 0, \\ \frac{\partial \sigma_{12}}{\partial x_1} + \frac{\partial \sigma_{22}}{\partial x_2} + f_2 &= 0, \\ \frac{\partial \sigma_{33}}{\partial x_3} + f_3 &= 0, \end{aligned} \right\} \quad (5)$$

one obtains a system of second-order PDEs for the fields u_1 , u_2 and T . In (5), the only nonzero component of the volume force is $f_2 = -\rho g$. The symbols ρ , g represent the material density and the gravitational constant, respectively. If all quantities are constant in the x_3 -direction (as in our case), then the last equation in (5) is satisfied automatically.

In addition to the equilibrium equations (5), we consider the stationary heat transfer equation

$$-\nabla \cdot (a \nabla T) = 0, \quad (6)$$

where the thermal conductivity a is a nonzero constant. These equations are assumed in a bounded polygonal domain $\Omega \subset \mathbb{R}^2$.

1.2 Boundary conditions

Let the boundary $\partial\Omega$ have nonempty open subsets $\Gamma_0, \Gamma_1, \Gamma_2$ and Γ_3 such that $\Gamma_0 \cap \Gamma_1 = \emptyset$ and $\Gamma_0 \cap \Gamma_2 = \emptyset$. Equations (5), (6) are equipped with boundary conditions of the form

$$\left. \begin{aligned} \sum_{j=1}^2 \sigma_{ij} \nu_j &= g_i^* \quad \text{on } \Gamma_0, \quad i = 1, 2, \\ u_1 &= u_1^* \quad \text{on } \Gamma_1, \\ u_2 &= u_2^* \quad \text{on } \Gamma_2, \\ T &= T^* \quad \text{on } \Gamma_3, \\ \frac{\partial T}{\partial \nu} &= T_N^* \quad \text{on } \partial\Omega \setminus \Gamma_3. \end{aligned} \right\} \quad (7)$$

Here $g_i^*, u_i^*, T^*, T_N^* \in L^2(\partial\Omega)$ are prescribed boundary force components, displacement components, temperature, and temperature flux, respectively (other standard types of boundary conditions may be used as well). The symbol ν stands for the unit outer normal vector to $\partial\Omega$.

1.3 Weak formulation

The solution u_1, u_2, T is sought in the form

$$u_1 = U_1 + \tilde{u}_1, \quad u_2 = U_2 + \tilde{u}_2, \quad T = \Theta + \tilde{\theta}, \quad (8)$$

where $U_1 \in V_1, U_2 \in V_2, \Theta \in V_3$. The function spaces are determined as usual by the boundary conditions (7): $V_1 = \{\varphi \in H^1(\Omega); \varphi = 0 \text{ on } \Gamma_1\}$, $V_2 = \{\varphi \in H^1(\Omega); \varphi = 0 \text{ on } \Gamma_2\}$, $V_3 = \{\varphi \in H^1(\Omega); \varphi = 0 \text{ on } \Gamma_3\}$. The Dirichlet lifts are defined as follows: $\tilde{u}_1 \in H^1(\Omega)$ is any function satisfying $\tilde{u}_1 = u_1^*$ on Γ_1 , $\tilde{u}_2 \in H^1(\Omega)$ is such that $\tilde{u}_2 = u_2^*$ on Γ_2 , and $\tilde{\theta} \in H^1(\Omega)$ satisfies $\tilde{\theta} = \theta^*$ on Γ_3 . Equations (5), (6) are formulated in the weak sense as usual and the resulting bilinear forms can be written in a 3×3 block structure,

$$\left. \begin{aligned} a_{11}(U_1 + \tilde{u}_1, \hat{u}_1) + a_{12}(U_2 + \tilde{u}_2, \hat{u}_1) + a_{13}(\Theta + \tilde{\theta}, \hat{u}_1) &= 0 \quad \forall \hat{u}_1 \in V_1, \\ a_{21}(U_1 + \tilde{u}_1, \hat{u}_2) + a_{22}(U_2 + \tilde{u}_2, \hat{u}_2) + a_{23}(\Theta + \tilde{\theta}, \hat{u}_2) &= 0 \quad \forall \hat{u}_2 \in V_2, \\ a_{33}(\Theta + \tilde{\theta}, \hat{\theta}) &= 0 \quad \forall \hat{\theta} \in V_3. \end{aligned} \right\} \quad (9)$$

The derivation of the forms a_{ij} from (5), (6) is elementary. The weak problem is stated as follows: Given the boundary conditions (7) and the Dirichlet lifts $\tilde{u}_1, \tilde{u}_2, \tilde{\theta}$, find $U_1 \in V_1, U_2 \in V_2$, and $\Theta \in V_3$ satisfying (9).

2 Multimesh hp -FEM

In order to capture individual behaviors of the solution components u_1, u_2, T more efficiently than standard hp -FEM, we approximate these fields on individual meshes τ_1, τ_2 and τ_3 , respectively. The meshes are generally unstructured and they consist of (possibly curved) quadrilateral and/or triangular elements. Mixed meshes containing both element types are allowed.

Ideally, the meshes τ_1, τ_2, τ_3 would be completely independent. However, for algorithmic reasons, we introduce a simplifying assumption that each of them is defined starting from a common coarse *master mesh* τ_m and a finite sequence of (mutually independent) elementary refinement operations. The master mesh τ_m is very coarse and it may not be used for discretization purposes. It serves as the top of a tree-like structure of meshes which is used by the multimesh assembling procedure. The situation is illustrated in Fig.1. Part E of Fig. 1 shows the geometrical union of all meshes in the system – we call it *union mesh* and denote by τ_u .

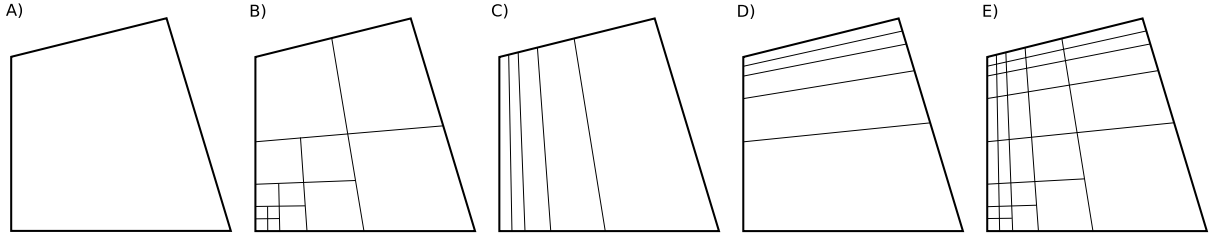


Figure 1: Example of a master mesh τ_m (A), meshes τ_1, τ_2, τ_3 obtained by its mutually independent refinements (B, C, D), and the corresponding union mesh τ_u (E).

2.1 Union mesh and the multimesh hp -FEM assembling procedure

The union mesh τ_u is never created physically, but its virtual elements guide the multimesh assembling algorithm. The algorithm visits all virtual elements of τ_u , determines the polynomial orders for all solution components, transforms the integration points, evaluates the corresponding contributions of the bilinear forms (9), and distributes the values into the stiffness matrix and right-hand side in a standard way. This is illustrated in Fig.2.

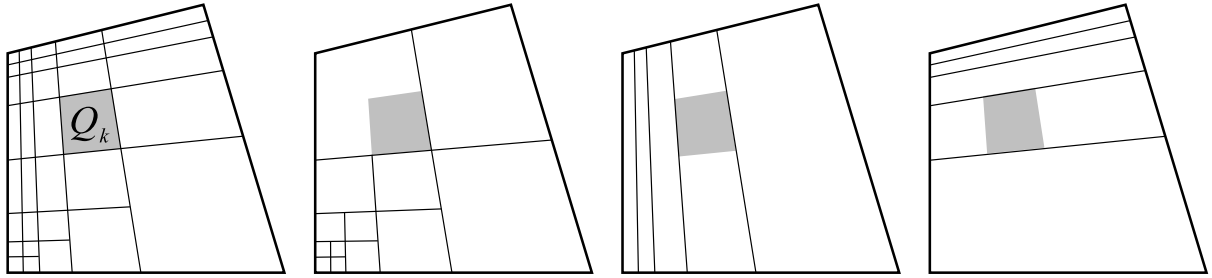


Figure 2: Virtual element Q_k of the union mesh τ_u and its counterparts in the meshes τ_1, τ_2 and τ_3 .

2.2 Integration over virtual elements

Consider a virtual element Q_k of the union mesh τ_u . In each mesh τ_i , there is exactly one element $K^{(i)}$ such that $Q_k \subset K^{(i)}$. In order to evaluate the bilinear forms a_{ij} in (9) on Q_k , we need to transform the elements $K^{(i)}$, $i = 1, 2, 3$ to the reference domain $K_q = (-1, 1)^2$. This is illustrated in Fig. 3.

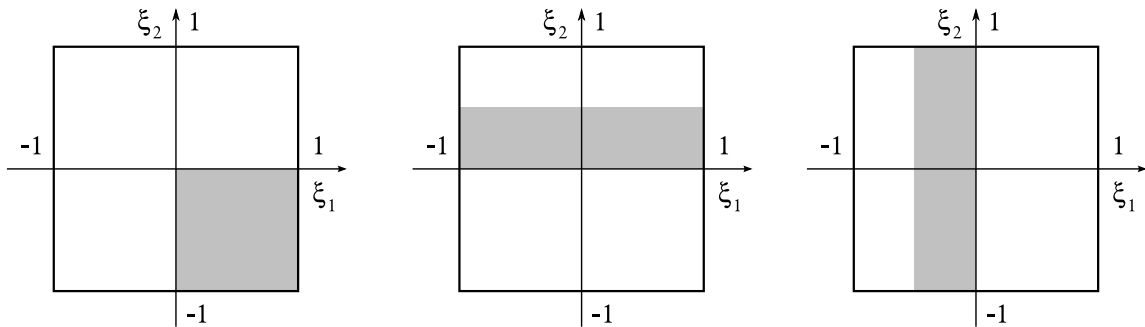


Figure 3: Elements $K^{(1)}, K^{(2)}, K^{(3)}$ of the meshes τ_1, τ_2 and τ_3 , containing Q_k , transformed to the reference domain K_q (cf. Fig. 2).

For any physical element $K = K^{(i)}$, the corresponding reference map is denoted by $\mathbf{x}_K : K_q \rightarrow K$. The reader can see that while $\mathbf{x}_K^{-1}(K) = K_q$, the virtual element $Q_k \subset K$ transforms to a subset $\mathbf{x}_K^{-1}(Q_k) \subset K_q$. Since the Gauss quadrature points and weights are defined on the *entire* reference

domain K_q , for each subset $\mathbf{x}_K^{-1}(Q_k)$ we need to introduce one more mapping $\mathbf{r}_K : K_q \rightarrow K_q$ such that $\mathbf{r}_K^{-1}(\mathbf{x}_K^{-1}(Q_k)) = K_q$. The situation is illustrated in Fig. 4.

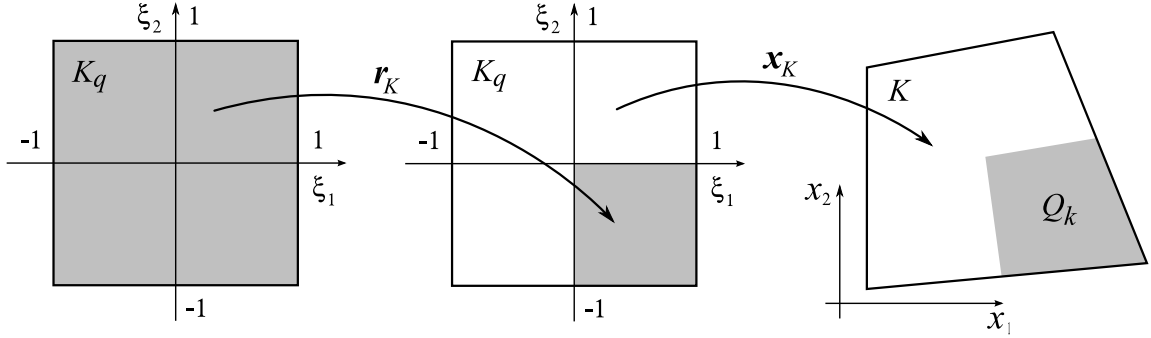


Figure 4: The mappings \mathbf{r}_K and \mathbf{x}_K .

Hence, for each virtual element $Q_k \subset K$ (the right-most part of Fig. 4), Gauss integration of sufficiently high order is performed on K_q (the left-most part of Fig. 4). Note that the mapping \mathbf{r}_K is affine of the form $\mathbf{r}_K(\boldsymbol{\xi}) = \mathbf{R}_K \boldsymbol{\xi} + \mathbf{t}_K$, and therefore its Jacobi matrix is diagonal. This fact greatly simplifies the computer implementation.

2.3 Automatic adaptivity in the multimesh hp -FEM

Automatic adaptivity algorithms for the hp -FEM have been discussed in numerous papers and monographs (see, e.g., [12, 13] and the reference therein). Therefore, we will only point out where automatic adaptivity for the multimesh hp -FEM is different.

In contrast to standard hp -FEM, the approximation error e_{hp} in the multimesh hp -FEM is a vector-valued function with the components $e_{1,hp}, e_{2,hp}, e_{3,hp}$ (corresponding to the fields u_1, u_2, T , respectively). The total error is measured in an energetic norm

$$\|e_{hp}\|_e^2 = \sum_{i=1}^3 \|e_{i,hp}\|_{i,e}^2, \quad (10)$$

where

$$\left. \begin{aligned} \|e_{1,hp}\|_{1,e}^2 &= a_{11}(e_{1,hp}, e_{1,hp}) + a_{12}(e_{2,hp}, e_{1,hp}) + a_{13}(e_{3,hp}, e_{1,hp}), \\ \|e_{2,hp}\|_{2,e}^2 &= a_{21}(e_{1,hp}, e_{2,hp}) + a_{22}(e_{2,hp}, e_{2,hp}) + a_{23}(e_{3,hp}, e_{2,hp}), \\ \|e_{3,hp}\|_{3,e}^2 &= a_{33}(e_{3,hp}, e_{3,hp}). \end{aligned} \right\} \quad (11)$$

For an element $K^{(i)} \in \tau_i$, the error value $\hat{e}^{(i)}$ is defined using the element contribution to the i th error component $\|\hat{e}_{i,hp}\|_{i,e}$. (Note that such splitting of error components is not possible in standard hp -FEM since one only has one mesh.) The elements of all three meshes τ_1, τ_2, τ_3 are then collected in a single list L and sorted according to their error values $\hat{e}^{(i)}$ in descending order. The rest of the procedure is the same as in standard hp -FEM.

3 Numerical experiments

We consider the cross-section of the winding of a massive coil with two cooling channels, as shown in Fig. 5. The material is heated by a current flowing through the winding and cooled by fluid running through the channels, whose temperature has stabilized at the value T_C . This causes a nonuniform temperature distribution in the winding and consequently thermoelastic deformations.

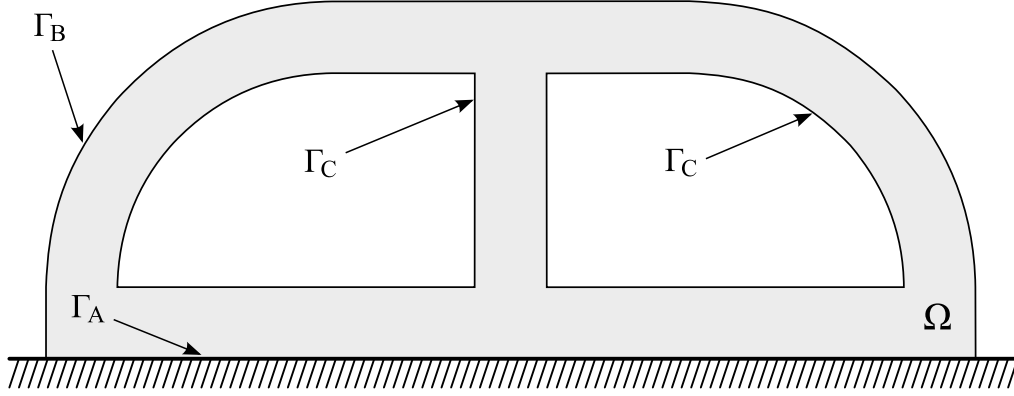


Figure 5: Transversal cross-section of the massive winding.

The transversal outer measures of the winding are $13L \times 5L$ and the cavities measure $5L \times 3L$. We prescribe zero displacement on Γ_A and zero external forces on the remaining part of the boundary $\Gamma_B \cup \Gamma_C$:

$$(u_1, u_2) = 0 \quad \text{on } \Gamma_A$$

$$\sum_{j=1}^2 \sigma_{ij} n_j = 0 \quad \text{on } \Gamma_B \cup \Gamma_C, \quad 1 \leq i \leq 2.$$

Here, $\mathbf{n} = (n_1, n_2)$ stands for the unit outer normal vector to the boundary $\partial\Omega$. For the thermal part, we prescribe a fixed temperature T_C on the face Γ_C , and a negative heat flux ϕ_B on the winding-air interface Γ_B :

$$T = T_C \quad \text{on } \Gamma_C,$$

$$\frac{\partial T}{\partial \mathbf{n}} = \phi_B < 0 \quad \text{on } \Gamma_B,$$

In computations whose results are presented below, we used the values $L = 0.1$, $T_C = 50$, $\phi_B = -50$, $\rho = 8000$, $g = 9.81$, $a = 1.3 \cdot 10^{-5}$, $E = 200$ GPa, $\nu = 0.3$ (data taken from [14]).

3.1 Comparison of standard and multimesh hp -FEM

The problem is first solved using standard hp -FEM that starts from the initial mesh shown in Fig. 6.

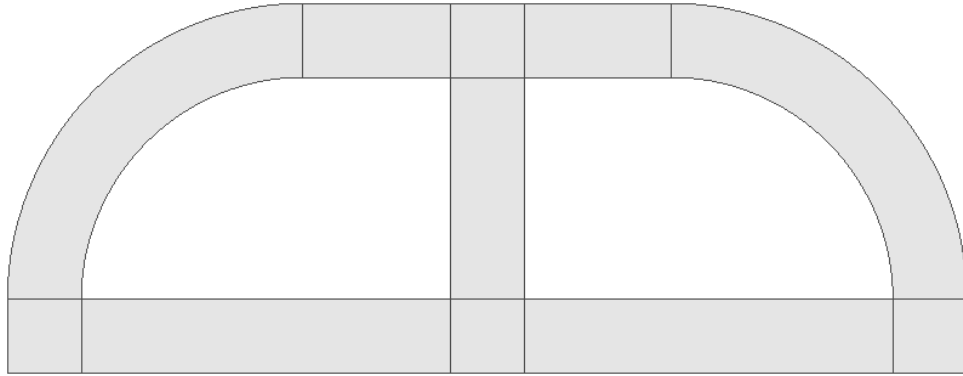


Figure 6: Initial mesh for standard hp -FEM (also master mesh for the multimesh hp -FEM). The circular arcs are represented by NURBS.

Figs. 7 and 8 show the corresponding stationary temperature and stress distributions.

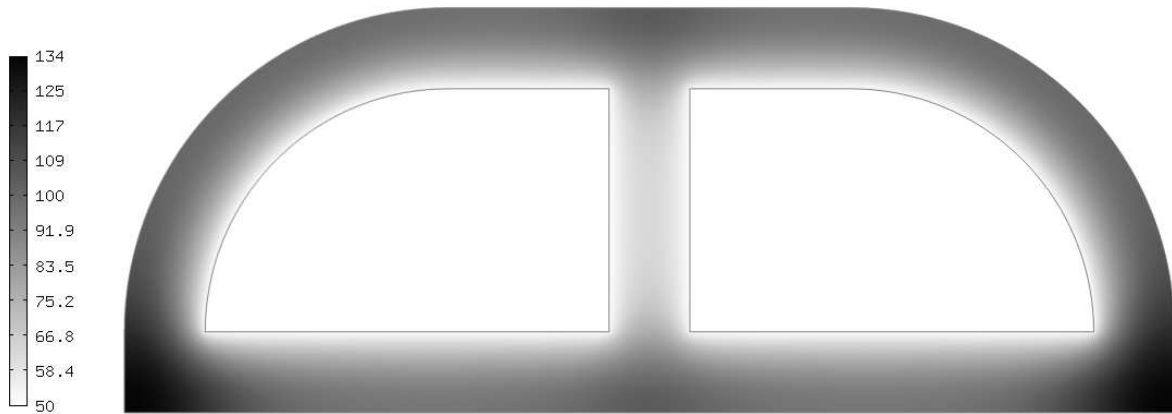


Figure 7: Temperature distribution.

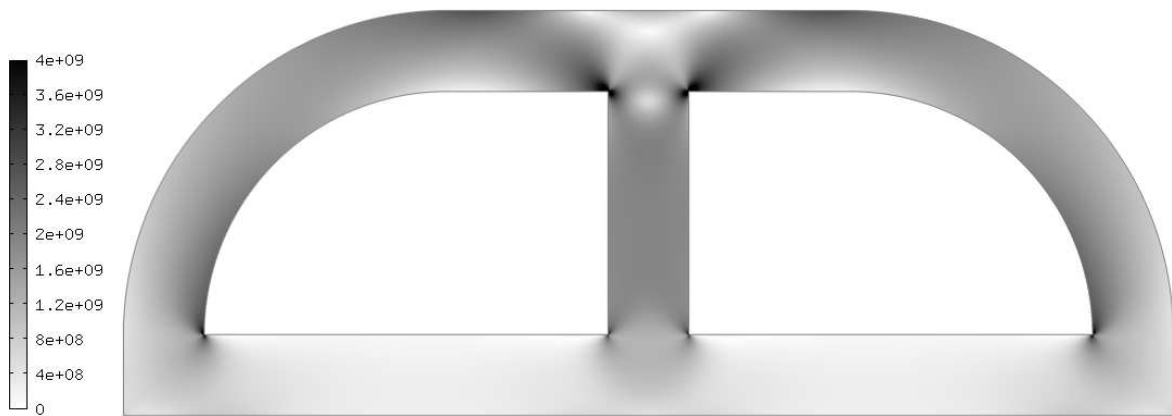


Figure 8: Stress distribution.

Fig. 9 shows the locally refined hp -mesh after 12 refinement steps. For reference, the numbers of DOF are 1542 for u_1 , 1539 for u_2 , and 1559 for T (total of 4640).

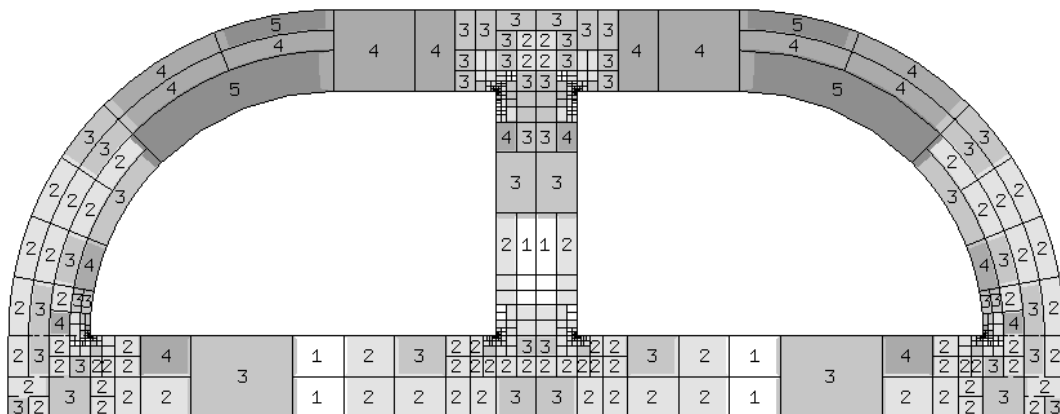


Figure 9: Standard hp -FEM mesh after 12 refinement steps. (The numbers inside elements stand for polynomial degrees.)

The master mesh for the adaptive multimesh hp -FEM is chosen to be identical to the starting mesh for the standard hp -FEM (Fig. 6). Meshes corresponding to the fields u_1, u_2 and T , at the same total error level as in the standard hp -FEM computation, are shown in Figs. 10 - 12. This time, the numbers of DOF for u_1, u_2 and T are 1309, 1602 and 205 (total of 3116). Thus the discrete problem size dropped to 67% compared to the standard hp -FEM. This is close to optimal given the fact that the fields u_1 and u_2 are very similar in nature, and thus most savings take place in the temperature field only. There, the number of DOF dropped from 1559 to 205 (13% compared to standard hp -FEM).

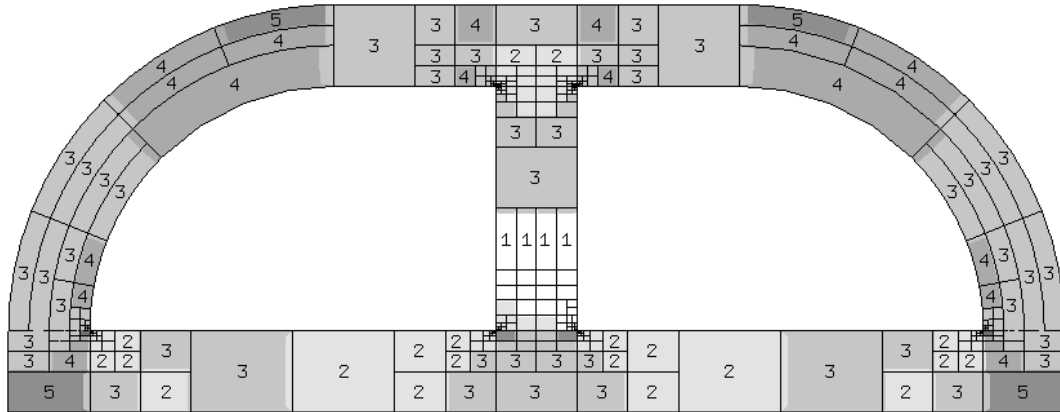


Figure 10: Multimesh hp -FEM: mesh for u_1 .

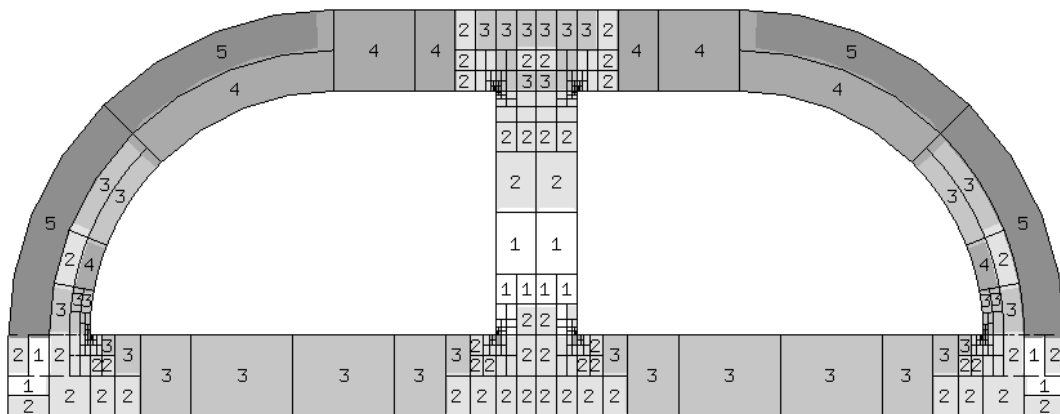


Figure 11: Multimesh hp -FEM: mesh for u_2 .

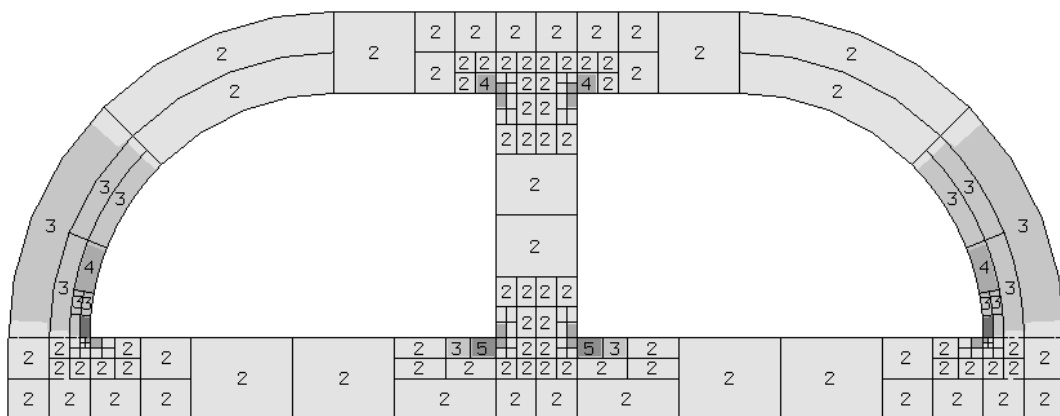


Figure 12: Multimesh hp -FEM: mesh for T .

Figs. 13 and 14 compare the performance of the hp -FEM (both single- and multimesh) with the h -FEM with quadratic elements in terms of the discrete problem size and CPU time requirements. Note that the scale on the vertical axis is logarithmic. In both cases, the multimesh hp -FEM was most efficient. This is a representative behavior that we have observed many times in various thermoelasticity computations. The computations were done using our open source hp -FEM library Hermes¹.

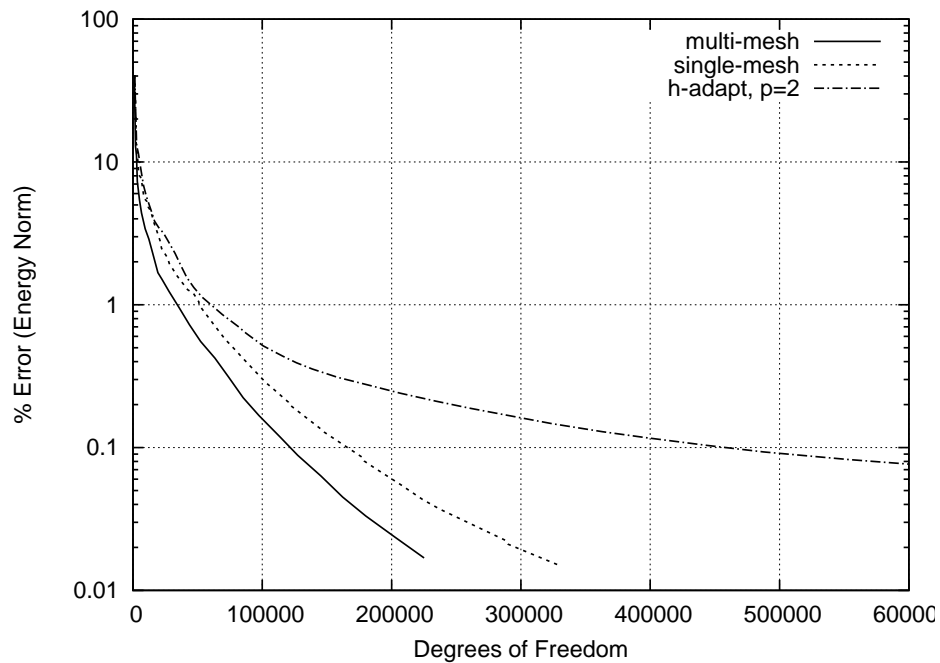


Figure 13: Comparison of the hp -FEM (single- and multimesh) and h -FEM with quadratic elements.

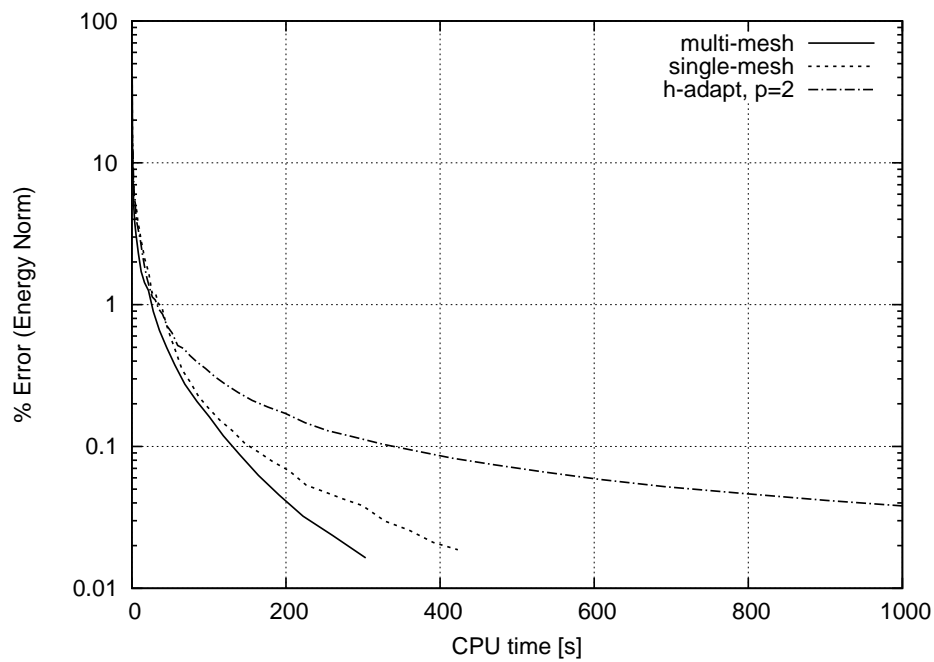


Figure 14: Comparison of CPU times.

¹<http://hpfem.org/>

4 Conclusion and outlook

We presented a novel adaptive multimesh hp -FEM technique for linear thermoelasticity problems where the displacements and the temperature were approximated on individual meshes equipped with mutually independent hp -adaptivity mechanisms. The design of this technique was driven by an effort to approximate efficiently a system of physical fields whose large qualitative differences make their approximation on a single mesh inefficient. Using different meshes for various physical fields is done quite often in operator splitting (OS) methods (let us only mention [10, 11] for all of them). However, these approaches are known to suffer from projection errors caused by transfer of functions between different meshes, which affect not only the accuracy but also stability of OS schemes. Our method is monolithic in nature and it avoids completely the problems associated with operator-splitting methods.

The numerical results confirmed that splitting the meshes indeed was a good idea: The mesh for the temperature remained relatively coarse in singular stress regions despite large amounts of local refinements occurred in the meshes for u_1 and u_2 . In practice, when a linear thermoelasticity problem exhibits singular stresses, the multimesh hp -FEM always outperforms the standard hp -FEM.

Currently, we are testing the adaptive multimesh hp -FEM on various multiphysics problems such as microwave and induction heating, heat and moisture transfer in concrete, and thermally conductive flow. We also found that this technique allows us to construct simple and very efficient space-time adaptive hp -FEM algorithms. Publications related to these topics are in preparation.

References

- [1] D. Iesan, A. Scalia. *Thermoelastic Deformations*, Springer, 1996.
- [2] A.M. Kosevich, E M Lifshitz, L D Landau, L. P. Pitaevskii. *Theory of Elasticity. Third Edition*, Butterworth-Heinemann, 1986.
- [3] J.E. Marsden, T.J.R. Hughes. *Mathematical Foundations of Elasticity*, Dover Publications, 1994.
- [4] S. Timoshenko. *Theory of Elasticity*, McGraw-Hill, 1970.
- [5] Z.P. Bazant et al. *Concrete at High Temperatures, Material Properties and Mathematical Models*, Longman, Essex, 1995.
- [6] P. C. Jain, M. N. G. Rao. Analysis of Steel Frames Under Fire Environment, *International Journal for Numerical Methods in Engineering* 19 (2005) 1467 - 1478.
- [7] T.T. Lie, R.J. Irwin. Method to Calculate the Fire Resistance of Reinforced Concrete Columns with Rectangular Cross Section, *ACI Structural Journal* 90 (1993) 52 - 60.
- [8] M.J. Terro. Numerical Modelling of the Behaviour of Concrete Structures in Fire, *ACI Structural Journal* 95 (1998) 183 - 193.
- [9] C. Miehe. Entropic Thermoelasticity at Finite Strains. Aspects of the Formulation and Numerical Implementation. *Computer Methods in Applied Mechanics and Engineering* Volume 120, Issues 3-4, 243-269, 1995.
- [10] D. Estep, S. Tavener, T. Wildey. A Posteriori Error Estimation and Adaptive Mesh Refinement for a Multi-Discretization Operator Decomposition Approach to Fluid-Solid Heat Transfer, submitted to Elsevier Science, 2008.
- [11] V. Mahadevan, J.C. Ragusa. Coupling Schemes for Multiphysics Reactor Simulation, INL report, INL/EXT-07-13490, (2007).
- [12] P. Solin, J. Cerveny, I. Dolezel. Arbitrary-Level Hanging Nodes and Automatic Adaptivity in the hp -FEM, *Math. Comput. Simul* 77 (2008), 117 - 132.
- [13] P. Solin, K. Segeth, I. Dolezel. *Higher-Order Finite Element Methods*, Chapman & Hall/CRC, Boca Raton, 2004.
- [14] Y.A. Cengel, R.H. Turner. *Fundamentals of Thermal-Fluid Sciences*, McGraw-Hill, 2005.